Catalytic conversion of 5-hydroxymethylfurfural (5-HMF) over Pd-Ru/FAU zeolite catalysts

Nathalia Ramírez Bocanegra[a], Javier Rivera De la Rosa[a], Carlos J. Lucio Ortiz[a], Pablo Cubillas González[b], Hugh Chris Greenwell[b] , Verónica E. Badillo Almaráz[c] , Ladislao Sandoval Rangel[d], Brenda Alcántar-Vázquez[e], Vicente Rodríguez-González[f], David Alejandro de Haro del Río[a*]

[a]Universidad Autónoma de Nuevo León, Facultad de Ciencias Químicas, Avenida Universidad S/N Ciudad Universitaria, San Nicolás de los Garza, Nuevo León, 64451, México
[b]Durham University, Department of Earth Sciences, Durham, DH1 3LE, United Kingdom
[c]Instituto Nacional de Investigaciones Nucleares ININ, Departamento de Sistemas Nucleares, México-Toluca S/N (km. 36.5), Edo. de México, 52750, México
[d]Tecnológico de Monterrey, Escuela de Ingeniería y Ciencias, Av. Eugenio Garza Sada 2501, Monterrey, Nuevo León,64849, México
[e] Instituto de Ingeniería, Universidad Nacional Autónoma de México, Avenida Universidad 3000, Coyoacán C.P. 04510, Cd. Mx., México
[f]Instituto Potosino de Investigación Científica y Tecnológica, División de Materiales Avanzados, Camino a La Presa de San José 2055, Lomas 4 sección, San Luis Potosí, S.L.P., C. P 78216, México

(*) corresponding author:
E-mail: david.dharodlr@uanl.edu.mx, Phone: +52 81 8329 4000

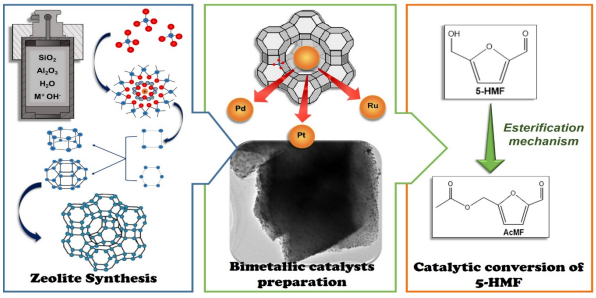

Abstract

We present this study on FAU-type zeolites were prepared varying the Si/Al ratio (4, 5 and 6) and crystallization time (4, 6 and 8 h) to produce a highly pure and homogeneous material with enhanced surface area values. Bimetallic Pd-Ru and Pt-Ru (0.5 wt.% of each metal) were impregnated onto the zeolites matrix by the incipient wetness impregnation method. The materials were characterized by X-ray diffraction (XRD), nitrogen physisorption, Fourier Transform Infrared spectroscopy (FT-IR), Scattering Electronic Microscopy (SEM), Scattering and Transmission Microscopy (STEM), temperature-programmed desorption (TPD), temperature-programmed desorption (TPR) and Inductively Couples Plasma- Mass Spectrometer (ICP-MS). Results indicated that using lower Si/Al ratios favored the catalytic activity. Also, the longest crystallization time had a positive effect on surface area, homogeneous particle size distribution and crystallinity. The catalytic performance in the esterification of 5-hydroxymethylfurfural (5-HMF) to produce 5-acetoxymethylfurfural (AcMF) was investigated. The maximum 5-HMF conversion of 87.28% was achieved using pure zeolite with relation Si/Al=5, and 8 h of crystallization. Pd-Ru supported onto same zeolite showed a conversion of 84.22%. The highest

selectivity towards AcMF of 71.29% with pure zeolite Si/Al=5 and 8 hours of crystallization was achieved, followed by Pd-Ru/FAU with Si/Al =5 and 8 hours of crystallization, achieving 60.42%. Finally, results shown that the interaction between the properties of zeolitic support and the metallic species, specifically Pd, had a positive effect in the catalytic process the pristine zeolite showed improved catalytic characteristics related to its acid strength.

Keywords: faujasite, hydrothermal synthesis, Si/Al ratio, 5-HMF, esterification

1. Introduction

The current growth of the population has led to an accelerated rate of industrial and technological development, increasingly demanding resources that come from non-renewable sources such as fossil fuels [1]. The indiscriminate consumption of these resources has produced serious and irreversible effects on the environment and human health, such as the increase of greenhouse gases in the atmosphere and climate change [2]. Additionally, the development of efficient, clean and environmentally friendly processes to produce high-value chemicals such as biofuels, fuel additives and chemical industry supplies, has been one of the main challenges worldwide in recent years [3]. An alternative feedstock that has been widely studied is lignocellulosic biomass, which is a renewable source for the production of a broad range of products such as biofuels and high-value products for the chemical industry [4,5]. The biomass represents a great potential, according to the International Energy Agency (IEA), that suggests that by 2035 the bioenergy will have the capacity to supply 10% of the world's primary energy and by 2050 biofuels can replace 27% of the fuel used in transportation [6]. Also, due to its high availability in nature, it is estimated that the global biomass production is around 100 billion tons per year, besides that it is a renewable source, and it does not generate new carbon dioxide to the atmosphere [7]. The lignocellulosic biomass is mainly composed for cellulose, hemicellulose and lignin, where carbohydrates of chains C_6 and C_5 as glucose, fructose, xylose, can be obtained directly from cellulose and hemicellulose [8], which are used as raw material in the synthesis of platform compounds such as 5-hydroxymethylfurfural (5-HMF) [9]. 5-HMF can be produced directly from the dehydration of fructose.

5-HMF is an aromatic aldehyde formed by a furanic ring, and an hydroxyl and carbonyl functional groups [10], which allow it to be the starting point of numerous chemical reactions to obtain a variety of high-value products, such as 5-acetoxymethylfurfural (AcMF), which can be obtained through esterification mechanism of 5-HMF. AcMF is a compound of great interest in industry in a wide range of applications as surfactants, fungicides, polymers and fuels production. AcMF presents an energetic density of 8.7 $kWhL^{-1}$, which is higher than ethanol (6.1 $kWhL^{-1}$) and similar

to gasoline (8.8 $kWhL^{-1}$) [11]. Furthermore, AcMF presents several advantages compared to 5-HMF in terms of industrial production, it is relatively more stable, less reactive, its recovery is simpler and cheaper and it can be used as reagent for the production of other added-value chemicals [12,13]. Through the years several processes for 5-HMF transformation have been developed, where heterogeneous catalytic processes have been widely researched. These processes present multiple advantages compared to other processes, in terms of selectivity, energetic requirements, easy recovery and reuse of the catalyst and low waste generation[14,15]. The catalyst synthesis has been the main focus of research for decades [16], where the aim is to improve the above mentioned properties, additionally, resistance to poisoning and favorable diffusion rates among others [17]. The performance of supported-metal catalysts is mainly defined by the inherent properties of the metal. Nevertheless, the support plays a key role during the reaction providing superior surface area and contributing to the catalyst dispersion [18]. Noble metals such as Pd, Ru and Pt have been widely used in catalytic reactions due to its chemical and structural stability along with electronic properties, noble metals allow to achieve high catalytic activities at less extreme conditions than with other transition metals[19][20]. Zeolites have a broad range of applications, particularly in heterogeneous catalysis as catalyst supports and have demonstrated to be a very versatile material with remarkable properties such as porosity, acidity and surface area. These properties are influenced by parameters such as atomic Si/Al atomic ratio, zeolites are composed by tetrahedra of $Si\text{-}O_4$ and $Al\text{-}O_4$, the presence of aluminum causes an charge disbalance in the framework that is compensated by a cation such as Na, and is directly related to the presence of acid sites [21]. Microporous zeolites have been used as catalyst in the transformation of molecules from biomass. Lanzafame *et al*. [22], studied the etherification reaction of 5-HMF, using H^+ and NH_4^+ modified mordenite (MOR), beta (BEA) and ZSM-5 zeolite types, to produce ethoxymethylfurfural (EMF), reaching a conversion of 100%. For biofuels production some studies have been reported, where faujasite (FAU) type zeolite has been widely used, due to its large cavity volume that facilitates the access to active centers [23], and low Si/Al ratio that allow it to have maximum ionic exchange capacity [24]. Recently, Perez-Bustos *et al*. [19] studied FAU type zeolite using structure directing agents (SDAs) and alumina as catalyst supports for bimetallic Pd-Ru and Pt-Ru with low metal content of 0.5 %, to obtain 2,5-DMF and AcMF hydrogenation and esterification products respectively, reaching 5-HMF conversion of 89% and up to 61% of selectivity to AcMF, this means that combinations of noble metals Pd-Ru and Pt-Ru are highly active at low concentrations. Also,

the production of AcMF from 5-HMF have been reported, Shinde *et al*. [13] studied the a cascade reaction to produce AcMF from glucose, with 5-HMF as a reaction intermediary, using Sn-Mont (Sn supported on montmorillonite clay) catalysts, reaching maximum 5-HMF conversion of 99% and 43% of selectivity to AcMF.

Characteristics of zeolites can be modified according to the synthesis method, obtaining suitable structural properties for each application [4]. There are several synthesis methods where templating, seed-assisted, dealumination and conventional hydrothermal methods can be highlighted, the aim of those methods is to favor the nucleation and the formation of mesoporosity in zeolites structure, which can improve diffusion rates during kinetic reactions. Templating method consists in the addition of large organic molecules to initial gel, that act as structure directing agent (SDA), crystal structure grows around the molecules and once the synthesis is finished, the SDA is eliminated by calcination, this is an expensive an pollutant method, nevertheless is used in most studies [25]. Si and al atoms are removed from zeolite structure in dealumination method, this is by a post-synthesis method that can affect chemical and thermal stability of zeolite structure [26]. In seed assisted nanometric crystals of interest zeolite are used to favor nucleation and formation of mesoporous zeolitic structures, the seeds are synthesized using different amounts of SDA [27]. Numerous efforts have been made to develop alternative template-free synthesis routes, by meticulous study of the factors involved in the synthesis such as the temperature and time of crystallization, Si/Al ratio, pH among others [28]. This research was focused on obtaining faujasite zeolite varying synthetic parameters without using SDAs, with remarkable properties of porosity and surface area. Also, bimetallic species were deposited onto the zeolite surface for comparison purposes. Materials were extensively characterized using XRD, FTIR, nitrogen physisorption, SEM, STEM, TPD and TPR including its evaluation in the esterification of 5-HMF for the AcMF production in order to correlate their properties with the performance in terms of conversion and selectivity.

2. Materials and methods

2.1. Catalysts Preparation

2.1.1. Zeolite Synthesis

A conventional hydrothermal synthesis was used to achieve the FAU type zeolite was followed according to [29]: (1) $Al(OH)_3 \cdot xH_2O$ (98%, Aldrich) as Al_2O_3 precursor was dissolved in a NaOH

(98%, Sigma-Aldrich) and deionized water solution. (2) Colloidal silica (Ludox HS-40, 40 wt%, Aldrich) as SiO_2 precursor was added to solution (1). The obtained gel was mixed up for 24 h under vigorous stirring (600 rpm). The resulted milky gel had an initial composition of $8Na_2O{:}xAl_2O_3{:}10SiO_2{:}400H_2O$ varying the Si/Al ratio (4,5 and 6). Then the gel was placed in a sealed teflon recipient and heated inside of an electric oven at 100 °C for 4, 6 and 8 h. The obtained powders were recovered by centrifugation, washed with deionized water and finally dried at 100 °C overnight. Samples were named as follows: Y-*z*-*x*h where, *z* is the Si/Al ratio (4, 5 or 6) and *x* is the crystallization time (4, 6 and 8 h).

2.1.2. Supported metallic catalysts preparation

The bimetallic particles of Pt-Ru and Pd-Ru were dispersed onto the prepared zeolitic supports following the incipient wetness impregnation (IWI) method. For the preparation of the Pd-Ru catalyst, 10.82 mg of palladium(II) nitrate hydrate ($Pd(NO_3)_2{\cdot}xH_2O$, Sigma Aldrich) and 10.26 mg of ruthenium(III) chloride hydrate ($RuCl_3{\cdot}xH_2O$, Sigma Aldrich) was dissolved in deionized water and added to the slurry. For Pt-Catalysts,13.26 mg of hexahydrate chloroplatinic acid ($H_2PtCl_6{\cdot}6H_2O$ ≥37.5% Pt basis, Sigma Aldrich) and ruthenium(III) chloride hydrate ($RuCl_3{\cdot}xH_2O$, Sigma Aldrich), was dissolved in 10 mL of H_2O and added to the slurry. The solutions were vigorously stirred during 24 h at room temperature, the resulting solid was recovered by filtration and dried overnight at 100 °C. The impregnated zeolites were then calcinated at 500 °C for 14 h with a heating ramp of 10 °C/min and 3 steps of 1 hour at 200 °C and 300 °C. Final materials were reduced at 550 °C in an inert atmosphere with 100 mL/min of H_2 30 %vol in N_2 for 3 h. The bimetallic catalysts were prepared with a nominal content of 0.5 wt% of each metal.

2.2. Catalysts characterization

X-ray diffraction (XRD) patterns were collected sing a Siemens D5000 diffractometer with CuK_α radiation (λ=1.5406 Å) operated at 35 kV and 25 mA in the 2θ range of 2–50° at 0.02°/min with a step time of 4 seconds. The average crystallite size (size of single crystal of zeolite) was estimated using the equation of Debye-Scherrer (Eq. 1).

$$D=k\lambda\cdot(\beta\cos\theta)^{-1} \qquad (1)$$

Where k is the dimensionless form factor (usually 0.94 for zeolites), D is the size of the crystallite in nm, λ is the wavelength of radiation of X-ray in CuK_α, β is the full width at half maximum (FWHM) of the diffraction peak and θ is the angle of the peak in the XRD pattern, the most

characteristic peak of crystalline phase of faujasite zeolite considered to obtain the crystallite size estimations was the peak at 6.8(2θ angle)[30]. Fourier transform infrared (FTIR) spectroscopy to identify the functional groups present on the surface of the zeolites was carried out. The analyses using a Perkin-Elmer instrument were performed, (Spectrum One model from 500 to 4000 cm^{-1} by diffuse reflectance using an attenuated total reflection (ATR) cell with 32 scans and a resolution of 4 cm^{-1}, KBr was employed as blank. The textural properties of the solids by the N_2 physisorption were assessed and the results were obtained from adsorption-desorption isotherms at -196 ºC using a Micromeritics Gemini 2360 pore analyzer. Prior to measurement, the samples were degassed during 4 h at 400 °C under vacuum. The specific superficial area was determined by the Brunauer, Emmet and Teller (BET) method. The external surface area (S_t) and micropore volume (V_{micro}) was determined by the t-plot method in the low-pressure range p/p_0 0.05 - 0.5, using de Boer's equation [31–33]. Total pore volume was estimated from desorption isotherm branch at p/p_0=0.98 assuming complete pore saturation. The pore size distribution was calculated by Barrett-Joyner-Halenda (BJH) method. The morphology was analyzed by scanning electron microscopy (SEM) using a Focused ion Beam (FIB) microscope, FEI Helios Nanolab 600 operating with acceleration voltage in the range of 350 V – 30 kV. The Si/Al molar ratio was determined by X-ray dispersive energy (EDX) using a HITACHI SU-70 microscope operating with acceleration voltage in the range of 0.5 – 30 kV, coupled to an EDX system X-Max^N 50 Silicon Drift Detector from OXFORD instruments. The distribution of metal particles over the zeolite surface was estimated by scanning and transmission electron microscopy (STEM) using a JEOL 2100F Field emission microscope with acceleration voltage of 200 kV, coupled to an EDX detector INCAx-sight from OXFORD Instruments. The acidity of the catalysts was determined by NH_3 temperature-programmed desorption (NH_3-TPD) tests using a Belcat B, from Bel Japan, equipped with a thermal conductivity detector (TCD). A NH_3–He gas mixture (Praxair Inc. Certified 5% mol concentration, in He balance) was employed as the analytical gas. In these TPD experiments, 100 mg of the samples were first pre-treated in He at 500 °C for 1 h, to clean the surface, and cooled to 50 °C. Then, the catalysts were exposed to NH_3-He flow (50 $mLmin^{-1}$) for 1h, purged with He and heated linearly at 10 °C min^{-1} over a temperature range of 50 - 600 °C in He gas flow (30 $mLmin^{-1}$). NH_3 in effluent gas was recorded continuously as a function of temperature with a TCD detector. The catalysts were subjected to temperature-programmed reduction (H_2-TPR) analysis to identify the reduction peaks that take place in the catalysts. ChemBET TPR/TPO Quantachrome equipment was used,

with a heating ramp of 10 °C/min, from 30 °C to 1000 °C and H_2 flow of 20 mL/min (10% H_2 in Ar). In order to quantify the final metallic load in the catalysts, they were analyzed by an inductively coupled plasma mass spectrometry (ICP-MS) instrument model Thermo Scientific XSeries 2.

2.3. Catalytic activity experiments

The catalytic reaction of 5-HMF esterification was carried out in a 250 mL glass reactor operated at atmospheric pressure, using a condenser and an oil bath as a heating medium. The reactor was loaded with a solution containing the different catalysts to be assessed (zeolite, Pd-Ru/zeolite or Pt-Ru/zeolite), 5-hydroxymethylfurfural (5-HMF 99 wt%, Fluorochem) with a weight ratio of catalyst/5-HMF of 2, formic acid (FA 96 wt%, Aldrich) with a weight ratio of catalyst/formic acid of 0.08, hydrochlorhydric acid (HCl ~37 wt%, Fisher scientific) with a weight ratio of catalyst/HCl of 1.42, and 20 mL of tetrahydrofuran (THF 99 %wt, Aldrich) as solvent, with a ratio of 0.1 g catalyst/20 mL solvent. The reactions were conducted at 70 °C, under atmospheric pressure, vigorous stirring at 400 rpm for 24 h, according to [19], for each catalyst the experiment was done for triplicate and average results are shown. The reaction products were centrifuged, recovered and cooled down before their characterization. The analysis and quantification of the reaction products by gas chromatography coupled to a mass spectrometer (GC-MS) was carried out using a Shimadzu QP2010-Ultra GC equipped with EI/CI quadrupole MS, EI is carried out at 70eV. Products were separated using a Rxi-5Sil MS column (0.15 μm x 10 m x 0.15 mm). THF was present in all the samples as solvent. The concentration of AcMF was calculated using the chromatograms, mass spectra from the National Institute of Standards and Technology (NIST) database [34].To better understand the catalytic activity, parameters such as 5-HMF conversion and AcMF selectivity were calculated according to Eq. 2 and 3.

$$\text{Conversion (\%)} = (n_{\text{5-HMF}} \text{ reacted}/n_{\text{5-HMF}} \text{ loaded})*100 \quad (2)$$

$$\text{Selectivity (\%)} = (n_{\text{AcMF}}/n_{\text{5-HMF}} \text{ reacted})*100 \quad (3)$$

3. Results and discussion

3.1. Catalysts characterization

The as-synthesized zeolites and supported bimetallic catalysts preparation were carried out as described in section **2.1.1**, and **2.1.2**. **Fig. 1** shows XRD patterns of FAU type zeolite synthesized

under different synthesis conditions of Si/Al ratio and crystallization time. Typical peaks corresponding to FAU zeolite can be observed according to the JCPDS card No. 039-1380 of octahedral faujasite zeolite [35]. Zeolites synthesized with Si/Al=5 and 6 presented a pure phase of faujasite type zeolite, whilst the zeolite synthesized with Si/Al=4 presented the characteristic peaks of FAU zeolite phase, besides a small peak around 8.6º corresponding to a levyne (LEV) type zeolite phase according to JCPDS card No. 51-0052 [36]. It is believed that Si/Al=4 ratio is in the lower limit of the crystallization field for the FAU phase [37]. For this reason, the FAUY zeolites Y-4-xh (Si/Al=4) were no further considered in the development of this work.

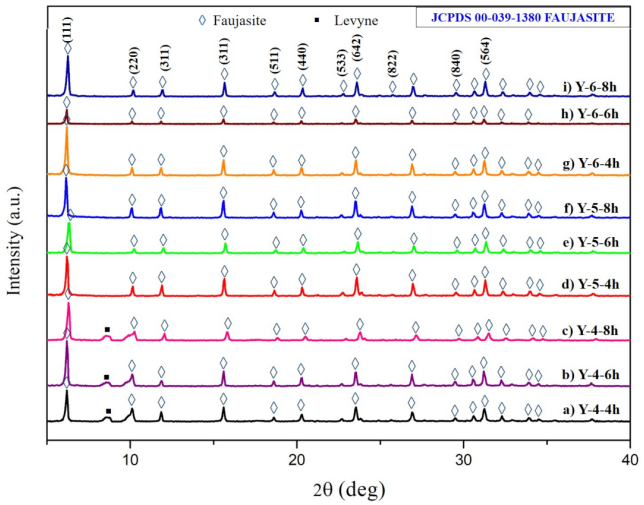

Fig. 1. XRD patterns of synthesized FAUY zeolite

The FTIR spectra of synthesized FAUY zeolites with relation Si/Al of 5 and 6 are presented in **Fig. 2**. These results show the characteristic faujasite bands that can be assigned to the asymmetric stretching of the tetrahedra TO_4 at 1102 - 991 cm^{-1}, symmetric stretching of the tetrahedra of S4R group is present at 776 - 709 cm^{-1}, there is also a weak shoulder around 900 cm^{-1}, which corresponds to ≡Al-OH bonds vibrations created by cation vacancies [38]. It is interesting to note that sample Y-5-8h is the only one presenting two peaks at 900 cm^{-1}, indicating the presence of ≡Al-OH bonds vibrations of two types, this can allow the deposition of metals on the surface of the material. The intrinsic water in the structure causes the broad band around 3000 - 3600 cm^{-1} corresponding to the stretching of linkages of OH groups, and the band around 1650 cm^{-1} corresponding to bending vibration of OH group [39].

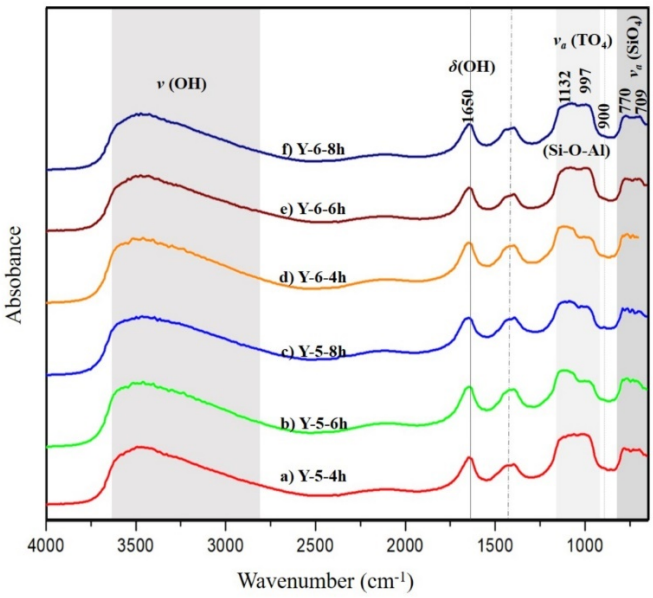

Fig. 2. FTIR spectra of synthesized FAUY zeolite

Nitrogen adsorption-desorption isotherms are presented in **Fig. 3.I,** All samples presented a typical behavior for microporous materials represented by an isotherm type I. Also, the isotherms show a small H3- type hysteresis loop, which indicates the formation slit-shaped pores, this shape has been also reported previously by Ramos *et al*. [40] for other nanostructured catalytic systems, and capillary condensation that represents the existence of mesopores in the structure of the material due to intercrystalline mesoporosity, the Si/Al= 5 seems to favor this behavior [37]. Few samples show an open hysteresis loop, although there is no vast literature describing this, [41] mentions that this kind of behavior can be related to aggregated materials having restricted mesopores that are not filled in the adsorption process.

Despite the presence of impregnated Pd-Ru and Pt-Ru metals on the surface of bimetallic catalysts, the BET surface area seems to be increased (around 10 %), this can be explained by the low concentration of metals that did not have influence on surface area. The increase of surface area could be explained by the calcination (at 500 °C) and subsequently reduction (at 550°C) stages prior to measurement, which were not carried out for pristine zeolites, those thermal treatments could favor the opening of zeolite pores [42].

Average pore size and volume was similar for all the catalysts, both bimetallic and zeolite without metals, ranging between 2.1 – 2-32 nm. The pore size distribution for all samples was carried out by the BJH method and it is shown in **Fig.3.II**. These results confirm that most of the pore volume

is within the microporosity range as all the samples show a sharp peak under 2 nm. In agreement with the isotherms, samples with Si/Al=5 have larger mesoporous volume than the Si/Al=6 materials. These results are in agreement with previous studies where at lower Si/Al ratios the zeolitic mesopore volume increases [43].

Also, the t-plot (not shown) analysis revealed that the range of micropore volume was 0.19 - 0.25 cm^3g^{-1} for all samples where the zeolite Y-6-6h presented the highest micropore volume (0.25 cm^3g^{-1}) and Y-6-4h the lowest (0.19 cm^3g^{-1}). The textural properties of synthesized zeolites are summarized in **Table 1**.

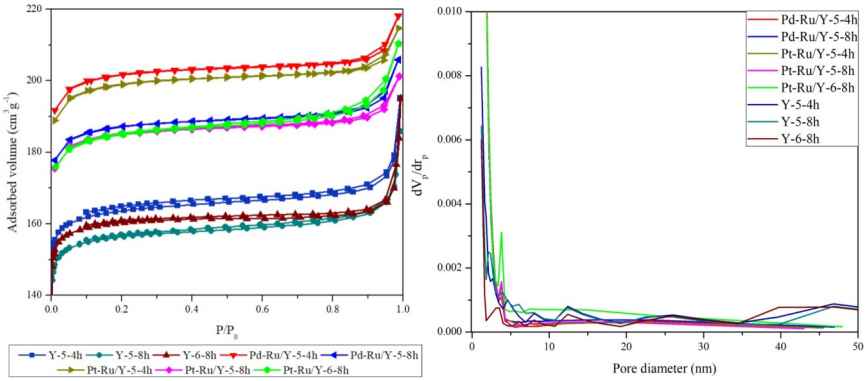

Fig. 3. I. N_2 adsorption-desorption isotherms and **II.** BJH pore size distribution of synthesized FAUY zeolite

From these results we can observe that there is a direct relation between the surface area of the material and the Si/Al ratio obtained by EDX (see **Table 1).** Surface area increases as Si/Al ratio does, this can be associated to that the empty volume also increases as Si/Al does due to the decrease of sodium cation that compensate the structure charge, and the decrease of water molecules in the pores asreported by Ahmedzeki *et al*. [44], where faujasite zeolite was synthesized by sol-gel method, surface areas around 201 - 299 m^2g^{-1} were obtained with the lowest studied Si/Al ratio. On the other hand, Ferdov *et al*. [45], obtained faujasite zeolite with surface areas above 800 m^2g^{-1}, the highest values for surface area were achieved with the highest possible for FAU Si/Al ratio (around 3).

Table 1. Properties of synthesized zeolite Y

Sample	[a]S_{BET} (m^2g^{-1})	[b]V_{Micro} (cm^3g^{-1})	[b]V_{Meso} (cm^3g^{-1})	[a]Pore diameter (nm)	[a]Total pore volume (cm^3g^{-1})	[c]Crystallite size (nm)	[d]Si/Al
Y-5-4h	562	0.24	0.059	2.14	0.30	62.43	1.98
Y-5-8h	537	0.23	0.048	2.12	0.28	69.27	1.78
Y-6-8h	550	0.24	0.051	2.12	0.29	58.75	1.83
Pd-Ru/Y-5-4h	603.4	--	--	2.23	0.337	--	--
Pd-Ru/Y-5-8h	560.6	--	--	2.27	0.318	--	--
Pt-Ru/Y-5-4h	630.7	--	--	2.1	0.332	--	--
Pt-Ru/Y-5-8h	555.1	--	--	2.24	0.311	--	--
Pt-Ru/Y-6-8h	558.8	--	--	2.32	0.325	--	--

[a]BET, [b]t-plot and [c]Debye-Sherrer's equation, [d]Calculated by EDX

SEM micrographs of Y-5-4h, Y-5-8h and Y-6-8h supports are presented in **Fig. 4**. These images indicate an increase in the average particle size with the increase of the crystallization time, i.e, zeolite Y-5-8h presented the highest particle size, around 718 nm. This is an expected behavior of the crystal growth [46]. Particle size distribution was analyzed using Image-J® software. Also, it is possible to observe that the octahedral morphology of all materials corresponds to faujasite type zeolite, it can be also noticed an intercrystalline growth and homogeneity of particles shape and size. EDX analysis was carried out to calculate Si/Al ratio for the chosen zeolites (Y-5-4h, Y-5-8h and Y-6-8h), these results are presented in **Table 1**, the values for calculated Si/Al ratio are in the range 1.78 – 1.98 and correspond to zeolite faujasite [47]. It can be seen a difference between Si/Al ratio of the initial precursor gel and calculated Si/Al ratio, due to the Si/Al of initial gel is the basis for the calculation of precursors used in the synthesis, and at the end of the synthesis remain some un-crystallized elements and the final Si/Al ratio changes [48].

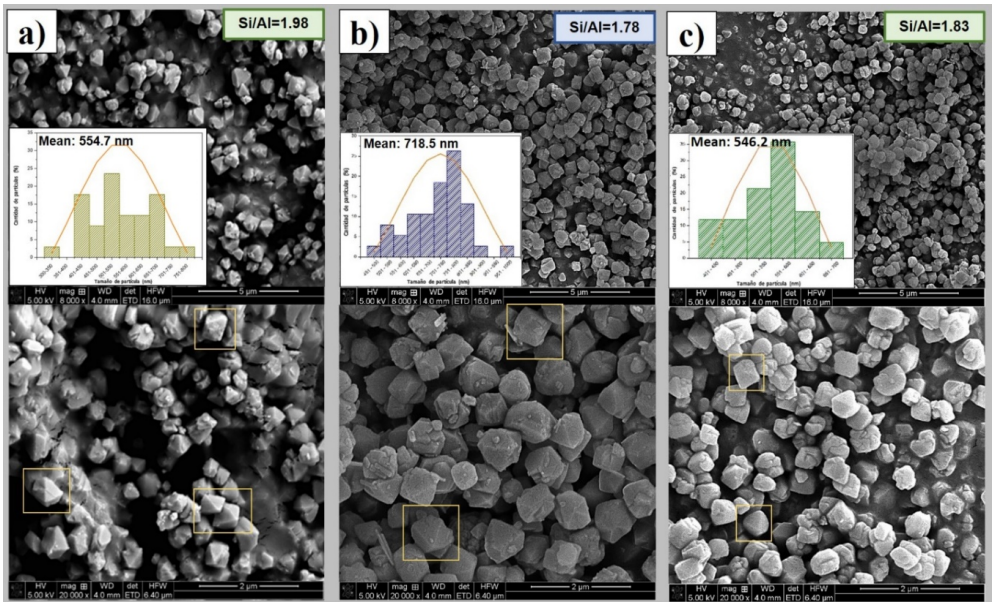

Fig. 4. SEM images of synthesized FAUY zeolite

In accordance to Kaneko *et al.* [49], when calcination is carried out under air atmosphere prior to reduction with H_2, there are two intermediary species during the process, $PtCl_4$ (200 - 300 °C) and $PtCl_2$ (300 – 325 °C), from 450 – 500 °C there is only Pt and Cl_2. This means that with this calcination temperature the Cl is completely removed from catalyst and the only impregnated specie is Pt. The nominal content of Pd-Ru and Pt-Ru in the supported-metal catalysts were designed to be 1 wt% (0.5 wt% for each metal) and the actual content was determined by ICP-MS and reported in **Table 2**.

Table 2. Metal loading of catalysts quantified by ICP-MS

Catalyst	Metal	Actual loading (wt%)
Pd-Ru/Y-5-4h	Pd	0.33
	Ru	0.09
Pt-Ru/Y-5-4h	Pt	0.01
	Ru	0.10
Pd-Ru/Y-5-8h	Pd	0.42
	Ru	0.15
Pt-Ru/Y-5-8h	Pt	0.01
	Ru	0.16
Pd-Ru/Y-6-8h	Pd	0.42
	Ru	0.09
Pt-Ru/Y-6-8h	Pt	0.02
	Ru	0.29

Pt-Ru catalysts presented highest weight loss for both Pt and Ru metals, where concentration of Ru

was higher than Pt. Loss of Pt in Pt-Ru catalysts can be explained by calcination temperature prior to reduction, according to Kaneko *et al.* [49], low Pt content requires lower calcination temperatures, otherwise the intermediary species ($PtCl_2$ and PtCl) can be easily volatilized, 350 °C seems to be enough to favor Pt dispersion for a metal content of 1 %, It is possible that with a metal content of 0.5% the calcination temperature could be even lower. On the other hand, Pd-Ru catalysts presented the lowest difference between the nominal and actual Pd concentration, thus the concentration of Pd was higher than Ru, differences in metal content can be attributed to impregnation method [50,51]. TEM has proved to be a powerful tool very useful to understand the structure-function relationship in zeolitic supports [52]. In **Fig. 5** and **Fig. 6** TEM micrographs of the Pd-Ru and Pt-Ru catalysts supported on zeolite Y-5-4h, Y-5-8h andY-6-8h are presented. The formation of metallic nanoparticles is observed, where clusters size is ranging from 14.8 nm to 36 nm. The metallic particles are relatively homogeneously distributed on the zeolitic supports. It is possible to observe that Pd-Ru/Y-5-8h catalyst showed a more favorable distribution of the metallic catalyst on the zeolitic surface. For Pt-Ru catalysts, the metallic particles distribution on the surface is less homogeneous than in Pd-Ru catalysts, besides, the presence if larger agglomerated nanoparticles can be observed. The metal distribution and the presence of agglomerated particles can be affected by several factors such as combination of morphological, physicochemical and structural properties of the zeolite Y-5-8h, characteristics of the metal particles and the impregnation method used.

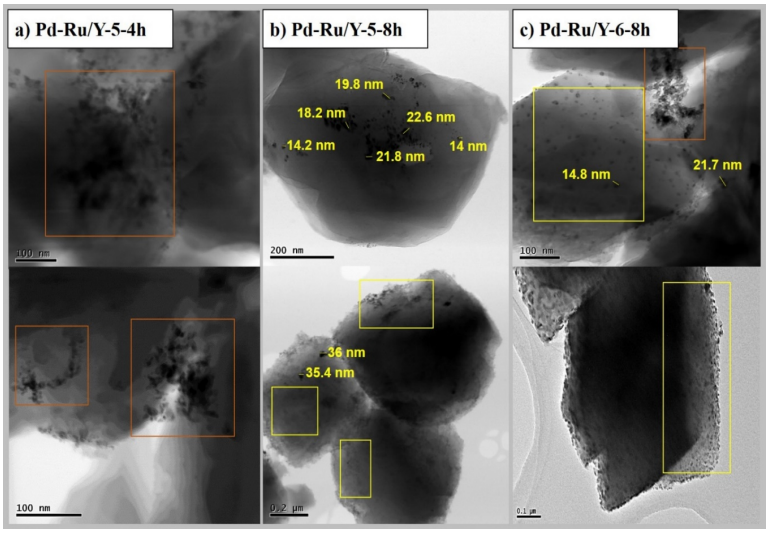

Fig. 5. TEM images of Pd-Ru catalysts supported on FAUY zeolite

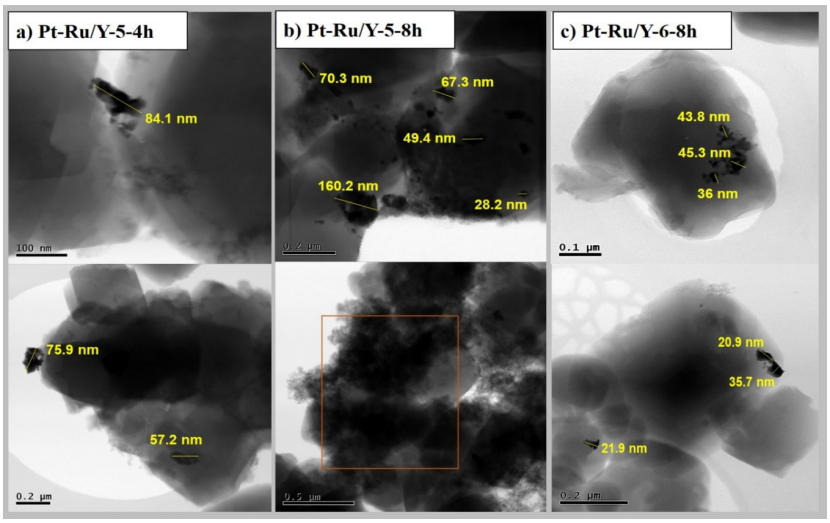

Fig. 6. TEM images of Pt-Ru catalysts supported on FAUY zeolite

Fig. 7. shows NH_3-TPD profiles of prepared catalysts. All materials show a very intense peak centered at 125 ºC and extended from 60 ºC to 350 °C, except Y-5-4h which shows a shift of the curve and reaches baseline at 400 °C. This peak showed a small shoulder peak at high temperatures around 250 ºC. According to Isernia [53] the desorption temperature range is correspondent to low-temperature zone 100-400 °C where the desorption peaks are attributed to weak and medium acid sites. The ammonia desorbed at low temperatures (T_D < 250 ºC) was ascribed to weak acidic sites, which correspond to physisorbed ammonia and partially ionic NH_4^+ bound to Brønsted acid site. The high temperature desorbed ammonia (250 < T_D < 400 ºC) was ascribed to desorption of coordinated NH_3 bound Lewis acid site [54]. Thermograms of catalysts with metallic species show a reduced amount of desorbed ammonia. These results are in agreement with those reported by Deng *et al*. [55] where an increase of exchanged cations reduced the acidity strength. The stronger and greater concentration of acidic sites of Y-5-4h can be then attributed to a higher extra-framework aluminum concentration [56]. Also, the additional thermal treatment for the metallic catalysts could have an effect on the decrease of acid sites.

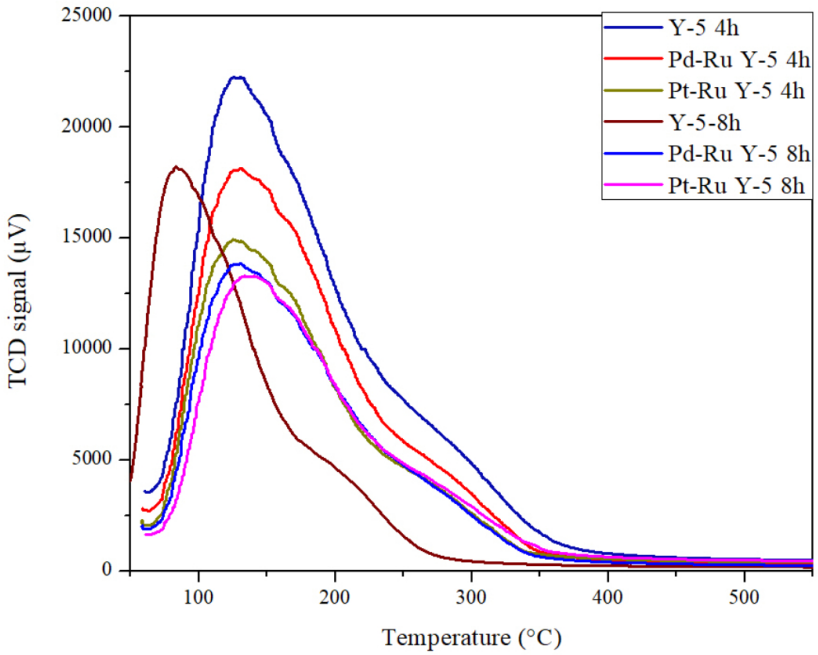

Fig. 7. NH_3-TPD profiles of zeolitic catalysts

Fig. 8. Shows H_2-TPR profiles for the different Pt-Ru and Pd-Ru/Y catalysts used in this work. It can be observed that the catalysts with Pt show very different reduction behavior compared with the catalysts with Pd. For Pt-Ru/Y-5-4h, one peak can be observed, between 75 and 175 °C, while for Pt-Ru/Y-5-8h, the same peak is shifted towards lower temperatures, between 50 and 160 °C. This may indicate a decreased dispersion of the metallic particles with increased crystallization time, probably due to the enhanced crystallinity of the FAU zeolite [57]. On the other hand, for Pd-Ru/Y catalysts, two peaks were observed. For Pd-Ru/Y-5-4h, the first peak is located between 50 and 150 °C, while the second peak is shown between 225 and 350 °C. With increasing crystallization time (Pd-Ru/Y-5-8h) an opposite effect is observed, now shifting the temperature of the peaks to the ranges of 125 – 150 °C and 350 – 450 °C. This may be explained due to a possible decrease in the particle size of Pd, which in turn would increase the interactions between Pd and the support. With increasing Si/Al ratio (Pd-Ru/Y-6-8h), temperatures shift even further, with the first peak being observed between 140 and 200 °C, and the second peak at 475 and 525 °C. While some works explain that increasing Si/Al ratios promote a decrease on reduction temperatures [58], it has also been shown that at higher Si/Al ratios, the relevance of the mesoporous volume increases, and a shift towards higher temperatures has been observed and attributed to metallic particles being located within the mesopores [59]. This is consistent also with

the fact that for the same crystallization time (8h), an increase in Si/Al from 5 to 6 also slightly enhances the mesopore volume (Table 1). Pt and Pd reduction peaks have been historically ascribed to temperatures within the range of 100 - 160 °C, while Ru peaks have been reported at 170 - 220 °C [19]. However, for our work, it seems the signals observed from the H_2-TPR experiments correspond to the reduction of PtO and PdO to Pt^0 and Pd^0, since the temperature ranges are very different from each other. The presence of additional peaks for Pd-Ru/Y-5-8h and Pd-Ru/Y-6-8h may provide evidence of a different interaction with the FAU support, forming a secondary phase with a stronger metal-support interaction [20].

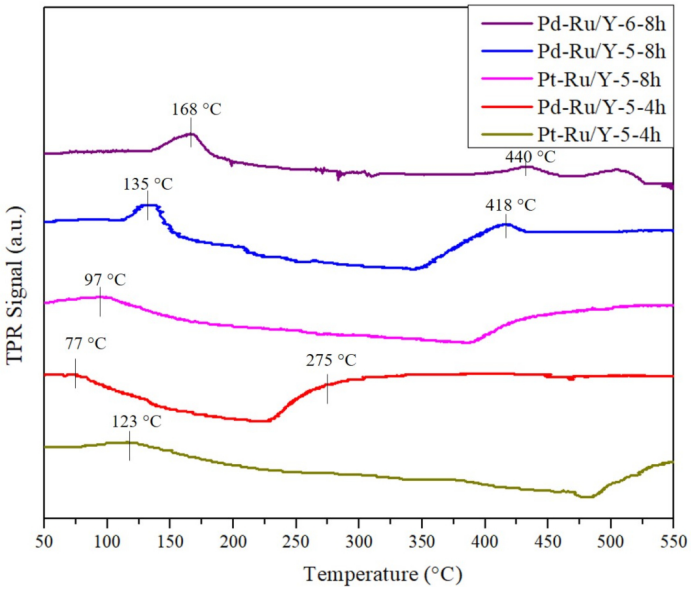

Fig. 8. H_2-TPR profiles of bimetallic catalysts

3.2. Catalytic activity experiments

In order to achieve the evaluation of the as-synthesized catalytic system a reaction of 5-HMF conversion and AcMF selectivity obtained from the catalytic experiments are shown in **Fig. 9**. The evaluated FAUY zeolites Y-5-4h, Y-5-8h and Y-6-8h showed high catalytic activity in the reaction of esterification of 5-HMF. The 5-HMF conversion for all the zeolites evaluated was above 85%. In the same way, all the evaluated catalysts, Pd-Ru and Pt-Ru supported on FAUY zeolites Y-5-4h, Y-5-8h and Y-6-8h; were found to be active in the esterification of 5-HMF. The conversion of HMF was ranging from 47.65 to 87.28%, and high selectivity to AcMF up to 71.29%, compared

to values reported by Shinde *et al*. [13], where a 43% yield of AcMF directly from glucose was achieved. A direct comparison between the different zeolites and bimetallic catalysts performance can be made, the highest conversion and selectivity with pure zeolite Y-5-8h were achieved (87.28% conversion and 71.29% selectivity) and with catalyst Pd-Ru/Y-5-8h (84.23% conversion and 60.42% selectivity). In most cases the zeolite structure is affected during the metallic supported catalyst preparation by IWI method, the pore channels probably adsorb metal precursors and in this occasion a blockage of the pore can take place decreasing the accessibility to active centers, acid sites density and surface area[60]. Although, the effect of Pd and Ru impregnation in the Pd-Ru/Y-5-8h catalyst did not decrease significantly the conversion and selectivity towards AcMF, and can be denoted that this catalyst kept a high quantity of Pd on surface (**Table 2**), Pérez *et al.*[19], did no report conversion using zeolite without metals, they achieved a conversion of 5-HMF of 61.72 % and a selectivity of 41.59 %, which is lower than reported in this study for Pd-Ru/Y-8h and Y-5-8h without metals.

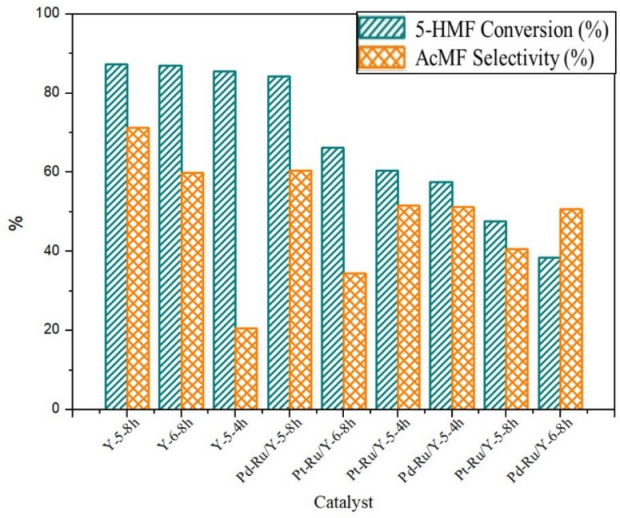

Fig. 9. 5-HMF conversion and AcMF selectivity with different catalysts

3.2.1. Effect of Si/Al ratio

The initial Si/Al ratio was varied (5 and 6) to study its effect in the 5-HMF conversions. In **Fig. 10.I**, the relation between 5-HMFconversion and Si/Al ratio of synthesized zeolites is reported, a similar behavior can be observed for the different evaluated catalysts, **Fig. 10.II**, shows the relation between 5-HMF conversion and Si/Al ratio (obtained by ICP-MS) of the bimetallic catalyst supported on zeolite. From these results, it can be noticed that there is not a lineal relationship

between these factors. Nevertheless, it is clear that the highest conversions were achieved with the lowest initial Si/Al ratio, i.e, zeolite Y-5-8h. When the amount of silicon atoms decrease, there is more place for aluminum atoms in zeolite structure, aluminum gives the acid character to the material due to its negative charge, so it could be derived in higher amount of acid sites, whose could be Brønsted site [61].

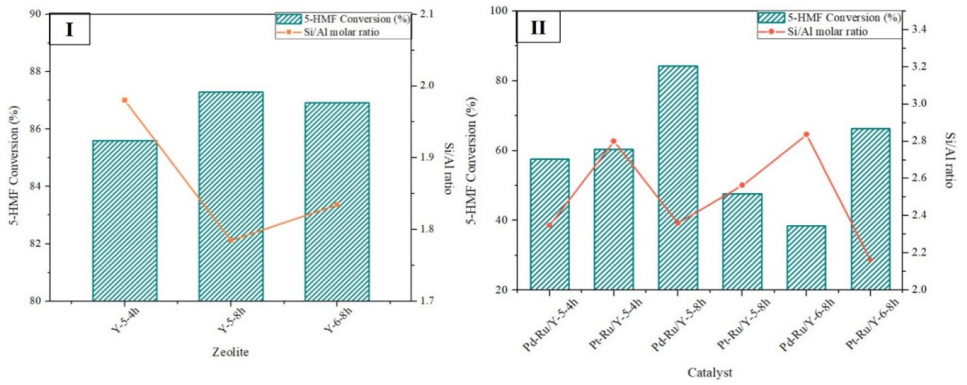

Fig. 10. I. Effect of Si/Al molar ratio on conversion of 5-HMF with zeolites as catalysts and **II.** Effect of Si/al molar ratio on conversion of 5-HMF with bimetallic catalysts supported on zeolite

3.2.2. Effect of metal loading

In **Fig. 11.** the relation between the 5-HMF conversion and metal content of the Pd-Ru and Pt-Ru catalysts is shown. It can be observed that in Pd-Ru catalyst, concentration of Pd is higher than Ru, the highest conversion was achieved with the highest content of both metals. For Pt-Ru catalyst, Ru concentration is higher than Pt, conversion seems to be favored by Ru content.

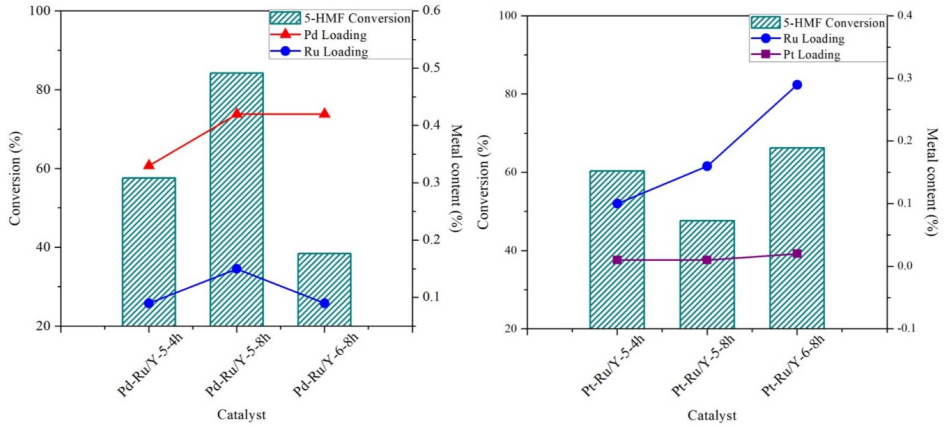

Fig. 11. Effect of metal content on conversion of 5-HMF, **I)** Pd-Ru catalysts and **II)** Pt-Ru catalysts

The main product identified from catalytic reaction was AcMF that is an esterification product, AcMF could be transform into biofuels as 2,5-dimehtylfuran (2,5-DMF) in a subsequent hydrogenation reaction. A proposal of reaction scheme to form AcMF is shown in **Fig. 12**, a reaction scheme can be explained as follows, having a concentration on HCl higher enough to produce H^+ ions in the reactive medium, that would promote esterification reaction by protonation of formic acid molecules that are attacked by the hydroxyl group of 5-HMF molecule.

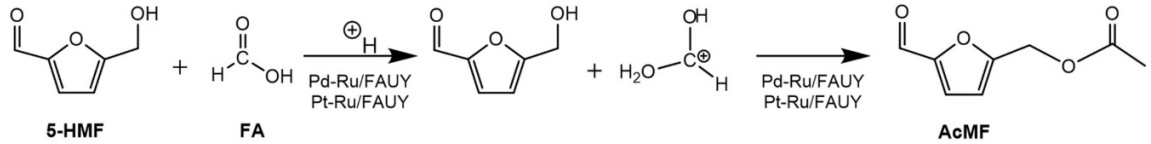

Fig. 127. Proposed reaction scheme

4. Conclusions

We present a successful synthesis of zeolitic materials and its extensive characterization including evaluation in the esterification of 5-HMF for the AcMF production. The results indicated well-defined structural, textural and morphological features as the characterization techniques indicated. At lower Si/Al ratio was favored the formation of mesopores in the materials achieving a material with combined microporous and mesopores to a lesser extent without the use of harmful SDAs. Moreover, a rise in the surface area values when Si/Al ratio increased was observed. Then, bimetallic Pd-Ru and Pt-Ru nanoparticles were also successfully supported and scattered on zeolites surface as resulted indicated. The Si/Al played a paramount role in the catalytic transformation of 5-HMF. A lower Si/Al ratio favored the catalytic activity of the material, presenting 87% in conversion and 71%in selectivity to AcMF. Besides, the supported catalysts Pd-Ru/Y-5-8h exhibited the highest catalytic activity, this could be explained by the inherent acidity of the zeolitic support and its synergy with Pd. However, the raw zeolite showed the highest catalytic activity both as a catalyst and as a catalyst support, this behavior can be attributed to the presence of stronger acid sites, porosity and structural characteristics of the material. Catalytic performance of bimetallic catalysts could be affected by pore channel blockage, loss of surface area and accessibility to acid sites due to the presence of the metallic particles.

5. Acknowledgements

This work was funded by Facultad de Ciencias Químicas, Universidad Autónoma de Nuevo León (UANL), Mexico. Authors wish to thank the Mexican Council for Science and Technology

(CONACyT) for scholarship of N. Ramírez-Bocanegra to the postgraduate studies in UANL (619679), and the internships at Durham University and Monterrey Institute of Technology and Higher Education (ITESM). We thank symposium organizers of F3: Advanced Catalytic Materials within framework of joint meeting between Sociedad Mexicana de Materiales and Materiales Research Society-USA for allowing to present our research results as well for the co-organization of the special issue.

References

[1] D. Kubička, I. Kubičková, J. Čejka, J.R. Cejka, Application of Molecular Sieves in Transformations of Biomass and Biomass-Derived Feedstocks, Catal. Rev. Sci. Eng. 55 (2013) 1–78. https://doi.org/10.1080/01614940.2012.685811.

[2] F.H. Sobrino, C.R. Monroy, J.L.H. Pérez, Biofuels and fossil fuels: Life Cycle Analysis (LCA) optimisation through productive resources maximisation, Renew. Sustain. Energy Rev. 15 (2011) 2621–2628. https://doi.org/10.1016/j.rser.2011.03.010.

[3] J. Roca Jusmet jordiroca, U. Stéphane Salaet Fernández, Agotamiento de los combustibles fósiles y emisiones de CO2: Algunos posibles escenarios futuros de emisiones, (2010).

[4] M. Acheampong, F.C. Ertem, B. Kappler, P. Neubauer, In pursuit of Sustainable Development Goal (SDG) number 7: Will biofuels be reliable?, Renew. Sustain. Energy Rev. (2016) 0–1. https://doi.org/10.1016/j.rser.2016.11.074.

[5] J.L. Toro-Trochez, E.S. Carrillo-Pedraza, D. Bustos-Martínez, F.J. García-Mateos, R.R. Ruiz-Rosas, J. Rodríguez-Mirasol, T. Cordero, Thermogravimetric characterization and pyrolysis of soybean hulls, Bioresour. Technol. Reports. 6 (2019) 183–189. https://doi.org/10.1016/J.BITEB.2019.02.009.

[6] Bioenergy, Int. Energy Agency. (n.d.).

[7] S. Wang, G. Dai, H. Yang, Z. Luo, Lignocellulosic biomass pyrolysis mechanism: A state-of-the-art review, Prog. Energy Combust. Sci. 62 (2017) 33–86. https://doi.org/10.1016/j.pecs.2017.05.004.

[8] C. Perego, A. Bosetti, Biomass to fuels: The role of zeolite and mesoporous materials, Microporous Mesoporous Mater. (2011). https://doi.org/10.1016/j.micromeso.2010.11.034.

[9] T. Ennaert, J. Van Aelst, J. Dijkmans, R. De Clercq, W. Schutyser, M. Dusselier, D. Verboekend, B.F. Sels, Potential and challenges of zeolite chemistry in the catalytic conversion of biomass, Chem. Soc. Rev. (2016). https://doi.org/10.1039/c5cs00859j.

[10] J.E. White, W.J. Catallo, B.L. Legendre, Biomass pyrolysis kinetics: A comparative critical review with relevant agricultural residue case studies, J. Anal. Appl. Pyrolysis. 91 (2011) 1–33. https://doi.org/10.1016/j.jaap.2011.01.004.

[11] Y. Zhang, J. Zhang, D. Su, 5-Hydroxymethylfurfural : A key intermediate for efficient biomass conversion, J. Energy Chem. 24 (2015) 548–551.

[12] L. Hu, L. Lin, Z. Wu, S. Zhou, S. Liu, Recent advances in catalytic transformation of biomass-derived 5-hydroxymethylfurfural into the innovative fuels and chemicals, Renew. Sustain. Energy Rev. 74 (2017) 230–257. https://doi.org/10.1016/j.rser.2017.02.042.

[13] S. Shinde, K. Deval, R. Chikate, Cascade Synthesis of 5- (Acetoxymethyl) furfural from Carbohydrates over Sn-Mont Catalyst, Chem. Sel. 3 (2018) 8770–8778. https://doi.org/10.1002/slct.201802040.

[14] C.M. Friend, Catálisis en superficies, Investig. Cienc. 201 (1993) 60–65.

[15] R.A. Sheldon, Green chemistry, catalysis and valorization of waste biomass, J. Mol. Catal. A Chem. 422 (2016) 3–12. https://doi.org/10.1016/j.molcata.2016.01.013.

[16] I. Arends, R. Sheldon, U. Hanefeld, I. Arends, U. Hanefeld, Introduction: Green Chemistry and

Catalysis, 2007. https://doi.org/10.1002/9783527611003.ch1.
[17] R. Srivastava, Synthesis and applications of ordered and disordered mesoporous zeolites: Present and future prospective, Catal. Today. 309 (2018) 172–188. https://doi.org/10.1016/j.cattod.2017.08.017.
[18] O. Terasaki, T. Ohsuna, What can we observe in zeolite related materials by HRTEM?, Catal. Today. 23 (1995) 201–218. https://doi.org/10.1016/0920-5861(94)00164-W.
[19] H. Fabio Pérez-Bustos, C.J. Lucio-Ortiz, J. Rivera De La Rosa, D.A. De Haro Del Río, L. Sandoval-Rangel, D. Xulú Martínez-Vargas, C. Solis Maldonado, V. Rodriguez-González, M.A. Garza-Navarro, F.J. Morales-Leal, C.P. 78216, Synthesis and characterization of bimetallic catalysts Pd-Ru and Pt-Ru supported on γ-alumina and zeolite FAU for the catalytic transformation of HMF, Fuel. 239 (2018) 191–201. https://doi.org/10.1016/j.fuel.2018.10.001.
[20] C.D. Taboada, J. Batista, A. Pintar, J. Levec, Preparation, characterization and catalytic properties of carbon nanofiber-supported Pt, Pd, Ru monometallic particles in aqueous-phase reactions, Appl. Catal. B Environ. (2009). https://doi.org/10.1016/j.apcatb.2008.12.016.
[21] G. Lemoine, Comparison of Different Types of Zeolites Used As Solid Acid Catalysts in Jatropha-Type Oil for Biodiesel, (2013) 1–183.
[22] P. Lanzafame, K. Barbera, S. Perathoner, G. Centi, E. Catizzone, G. Giordano, Comparison of H + and NH 4 + forms of zeolites as acid catalysts for HMF etherification, Catal. Today. 304 (2018) 97–102. https://doi.org/10.1016/j.cattod.2017.08.004.
[23] F.J. Luna, U. Schuchardt, Modificação de zeólitas para uso em catálise, Quim. Nova. 24 (2001) 885–892. https://doi.org/10.1590/S0100-40422001000600027.
[24] J.M. Gomez Martin, Síntesis, caracterización y aplicaciones catalíticas de zeolitas básicas, 2001.
[25] Y. Wang, Q. Wu, X. Meng, F.S. Xiao, Insights into the Organotemplate-Free Synthesis of Zeolite Catalysts, 3 (2017) 567–574. https://doi.org/10.1016/J.ENG.2017.03.029.
[26] E. Koohsaryan, M. Anbia, Nanosized and hierarchical zeolites : A short review, J. Catal. 37 (2016) 447–467. https://doi.org/10.1016/S1872-2067(15)61038-5.
[27] Q. Mou, N. Li, S. Xiang, Seed-directed synthesis of EMT-type zeolite from an organic-template-free system, Microporous Mesoporous Mater. 212 (2015) 73–79.
[28] M. Hartmann, Hierarchical zeolites: A proven strategy to combine shape selectivity with efficient mass transport, Angew. Chemie - Int. Ed. 43 (2004) 5880–5882. https://doi.org/10.1002/anie.200460644.
[29] P. Sharma, M.H. Han, C.H. Cho, Synthesis of zeolite nanomolecular sieves of different si/al ratios, J. Nanomater. 2015 (2015) 1–9. https://doi.org/10.1155/2015/912575.
[30] M. Khatamian, A. Yavari, A. Akbarzadeh, E. Alizadeh, Synthesis and characterization of MFI-type borosilicate zeolites and evaluation of their ef fi ciency as drug delivery systems, Mater. Sci. Eng. C. 78 (2017) 1212–1221. https://doi.org/10.1016/j.msec.2017.03.008.
[31] C.L.M. Rojas, Diseño y síntesis de materiales “a medida” mediante el método sol-gel, 2012.
[32] Y. Zheng, Evaluation of a New Method to Estimate the Micropore Volume and External Surface Area of Single-walled Carbon Nanotubes, The university of Tennessee, Knoxville, 2008.
[33] O.M. Sadek, S.M. Reda, R.K. Al-Bilali, Preparation and Characterization of Silica and Clay-Silica Core-Shell Nanoparticles Using Sol-Gel Method, Adv. Nanoparticles. 02 (2013) 165–175. https://doi.org/10.4236/anp.2013.22025.
[34] National Institute of Standards and Technology, Mass Spectra, in: P.J. Linstrom, W.G. Mallard (Eds.), NIST Chem. WebBook, NIST Stand. Ref. Database Number 69, NIST Mass Spec Data Center, S.E. Stein, director, Gaithersburg MD, 20899, 2018. https://doi.org/doi:10.18434/T4D303.
[35] C. Baerlocher, L.B. McCusker, D.H. Olson, Atlas of zeolite framework types, 6th ed., Elsevier B.V., Amsterdam, London, New York, Oxford, Paris, Shannon, Tokio, 2007. https://doi.org/10.1016/B978-044453064-6/50287-5.
[36] X. Zhao, W. Duan, Q. Wang, D. Ji, Y. Zhao, G. Li, Microwave-assisted ionothermal synthesis of Fe-LEV molecular sieve with high iron content in low-dosage of eutectic mixture, Microporous Mesoporous Mater. 275 (2019) 253–262. https://doi.org/10.1016/j.micromeso.2018.09.005.

[37] T.F. Chaves, H.O. Pastore, D. Cardoso, A simple synthesis procedure to prepare nanosized faujasite crystals, Microporous Mesoporous Mater. 161 (2012) 67–75. https://doi.org/10.1016/j.micromeso.2012.05.022.
[38] K. Byrappa, B. V. Suresh Kumar, Characterization of Zeolites by Infrared Spectroscopy, Asian J. Chem. 19 (2007) 4933–4935.
[39] S.M. Auerbach, K.A. Carrado, P.K. Dutta, Handbook of zeolite science and technology, 1st editio, CRC Press, Boca Raton, 2003.
[40] M. Ramos, F. Galindo-Hernández, I. Arslan, T. Sanders, J.M. Domínguez, Electron tomography and fractal aspects of MoS2 and MoS2Co spheres, Sci. Rep. 7 (2017) 1–9. https://doi.org/10.1038/s41598-017-12029-8.
[41] D.P. Lapham, J.L. Lapham, Gas adsorption on commercial magnesium stearate: The origin of atypical isotherms and BET transform data, Powder Technol. 342 (2019) 676–689. https://doi.org/10.1016/j.powtec.2018.10.035.
[42] K. Menad, A. Feddag, K. Rubenis, Synthesis and study of calcination temperature influence on the change of structural properties of the LTA zeolite, Rasayan J. Chem. 9 (2016) 788–797.
[43] Y. Gao, B. Zheng, G. Wu, F. Ma, C. Liu, Effect of the Si/Al ratio on the performance of hierarchical ZSM-5 zeolites for methanol aromatization, RSC Adv. 6 (2016) 83581–83588. https://doi.org/10.1039/c6ra17084f.
[44] N. s. Ahmedzeki, S. Yilmaz, B.A. Al-Tabbakh, Synthesis and characterization of the nanocrystalline zeolite Y, Al-Khwarizmi Eng. J. 12 (2016) 79–89. https://doi.org/10.1088/1757-899X/17/1/012030.
[45] S. Ferdov, K. Tsuchiya, N. Tsunoji, T. Sano, Comparative study between high-silica faujasites (FAU) from organic-free system and the commercial zeolite Y, Microporous Mesoporous Mater. (2018). https://doi.org/10.1016/j.micromeso.2018.09.036.
[46] M. Severance, Y. Zheng, E. Heck, P.K. Dutta, Influence of crystallite size on cation conductivity in faujasitic zeolites, J. Phys. Chem. A. 117 (2013) 13704–13711. https://doi.org/10.1021/jp407751d.
[47] A.G. Pelmenschikov, E.A. Paukshtis, M.O. Edisherashvili, G.. Zhidomirov, On the Loewenstein rule and mechanism of zeolite dealumination, J. Phys. Chem. 96 (1992) 7051–7055. https://doi.org/DOI: 10.1021/j100196a039.
[48] V.P. Valtchev, K.N. Bozhilov, Transmission Electron Microscopy Study of the Formation of FAU-Type Zeolite at Room Temperature, J. Phys. Chem. B. 108 (2004) 15587–15598. https://doi.org/10.1021/jp048341c.
[49] S. Kaneko, M. Izuka, A. Takahashi, M. Ohshima, H. Kurokawa, H. Miura, Pt dispersion control in Pt/SiO 2 by calcination temperature using chloroplatinic acid as catalyst precursor, Appl. Catal. A Gen. 427–428 (2012) 85–91. https://doi.org/10.1016/j.apcata.2012.03.033.
[50] G. Jacobs, F. Ghadiali, A. Pisanu, A. Borgna, W.E. Alvarez, D.E. Resasco, Characterization of the morphology of Pt clusters incorporated in a KL zeolite by vapor phase and incipient wetness impregnation . Influence of Pt particle morphology on aromatization activity and deactivation, 188 (1999) 79–98.
[51] E. del Río, D. Gaona, J.C. Hernández-garrido, J.J. Calvino, M.G. Basallote, M.J. Fernández-trujillo, J.A. Pérez-omil, J.M. Gatica, Speciation-controlled incipient wetness impregnation : A rational synthetic approach to prepare sub-nanosized and highly active ceria – zirconia supported gold catalysts, J. Catal. 318 (2014) 119–127.
[52] Á. Mayoral, P. del Angel, M. Ramos, Electron Microscopy Techniques to Study Structure/Function Relationships in Catalytic Materials, in: Adv. Catal. Mater. Curr. Status Futur. Prog., Springer International Publishing, 2019: pp. 97–128. https://doi.org/10.1007/978-3-030-25993-8_5.
[53] L.F. Isernia, FTIR study of the relation, between extra-framework aluminum species and the adsorbed molecular water, and its effect on the acidity in ZSM-5 steamed zeolite, Mater. Res. (2013). https://doi.org/10.1590/S1516-14392013005000044.
[54] A. Auroux, Calorimetry and Thermal Methods in Catalysis, 1st editio, Springer Berlin Heidelberg,

2013.
[55] C. Deng, J. Zhang, L. Dong, M. Huang, B. Li, G. Jin, J. Gao, F. Zhang, M. Fan, L. Zhang, Y. Gong, The effect of positioning cations on acidity and stability of the framework structure of y zeolite, Sci. Rep. (2016). https://doi.org/10.1038/srep23382.
[56] D. Jin, B. Zhu, Z. Hou, J. Fei, H. Lou, X. Zheng, Dimethyl ether synthesis via methanol and syngas over rare earth metals modified zeolite Y and dual Cu-Mn-Zn catalysts, Fuel. (2007). https://doi.org/10.1016/j.fuel.2007.03.011.
[57] X. Zhang, D. Tang, M. Zhang, R. Yang, Synthesis of NaX zeolite: Influence of crystallization time, temperature and batch molar ratio SiO2/Al2O3 on the particulate properties of zeolite crystals, Powder Technol. (2013). https://doi.org/10.1016/j.powtec.2012.10.046.
[58] J. Guo, W. Yang, Y. Zhang, L. Gan, C. Fan, J. Chen, Y. Peng, J. Li, A multiple-active-site Cu/SSZ-13 for NH3-SCO: Influence of Si/Al ratio on the catalytic performance, Catal. Commun. (2019) 105751. https://doi.org/10.1016/j.catcom.2019.105751.
[59] I. Graça, M.C. Bacariza, D. Chadwick, Glucose isomerisation into fructose over Mg-impregnated Na-zeolites : In fl uence of zeolite structure, Microporous Mesoporous Mater. 255 (2018) 130–139. https://doi.org/10.1016/j.micromeso.2017.07.015.
[60] Y. Shi, E. Xing, K. Wu, J. Wang, M. Yang, Y. Wu, Recent progress on upgrading of bio-oil to hydrocarbons over metal/zeolite bifunctional catalysts, Catal. Sci. Technol. 7 (2017) 2385–2415. https://doi.org/10.1039/C7CY00574A.
[61] A. Simon-Masseron, J.P. Marques, J.M. Lopes, F.R. Ribeiro, I. Gener, M. Guisnet, Influence of the Si/Al ratio and crystal size on the acidity and activity of HBEA zeolites, Appl. Catal. A Gen. 316 (2007) 75–82. https://doi.org/10.1016/j.apcata.2006.09.022.